Formation of chromium borides in quenched modified 310 austenitic stainless steel.

T. Sourmail, T. Okuda and J. E. Taylor

Department of Materials Science and Metallurgy, University of Cambridge

Pembroke Street, Cambridge CB2 3QZ, U.K.

Scripta Mater. **50***:2004, 1271-1276*

Boron segregation and precipitates were investigated using EFTEM. Chromium borides were identified. Comparison with published results suggests that segregation is mainly of non-equilibrium type. Non-uniform distribution of precipitates can be explained using nucleation theory if the segregation leads to grain-boundary boron concentration only slightly above the solubility limit.

1 Introduction

The beneficial effect of boron on the mechanical properties of austenitic stainless steels is well documented [1, 2]. A number of studies have confirmed that boron segregates to grain boundaries, in a variety of steels and nickel-base alloys (for example, [3, 4, 5]). Segregation of boron is known to occur via two mechanisms (for example, [1]):

Equilibrium segregation is caused by the high binding energy for boron at grain boundaries and other defects. This effect decreases with increasing temperature and depends strongly on the grain boundary structure.

Non-equilibrium segregation is caused by the dissociation of boron-vacancy complexes near the grain boundary which acts as a vacancy sink. In this case, the segregation effect increases as the starting temperature increases, and is believed to depend little on the nature of the grain boundary, as most are believed to be efficient vacancy sinks [6] (with the exception of twin boundaries, along which boron segregation is not observed).

The present study is concerned with segregation of boron and precipitation occurring in a modified type 310 austenitic stainless steel (20 wt% Ni, 25 wt% Cr), during quenching from high-temperature solution treatment. Although precipitation of borides or boro-carbides can be beneficial to creep properties, type 310 austenitic steel is primarily designed for use in highly corrosive environments. In this context, precipitation of borides or boro-carbides is undesirable. This is because, on one hand, the beneficial role of boron on hot workability is caused by boron in solid solution [1], and on the other hand, precipitation of chromium rich boro-carbides may result in sensitisation of the grain boundaries.

Precipitation of borides has not been systematically observed in boron containing steels [7, 4], and it was therefore not evident that the results of the detailed investigation by Karlsson *et al.* [3, 7, 8, 9] for a type 316 austenitic stainless steel (17 wt% Cr-13 wt% Ni) would apply to the type 310 investigated here.

2 Experimental procedures

2.1 Material and heat-treatment

The ingot of modified AISI 310 was produced using electric arc melting and vacuum-oxygen decarburisation process, then rolled into blooms, which were turned into seamless stainless tubes using hot extrusion. Small diameter tubes were obtained by cold-drawing. Their compositions are indicated in table 1.

All tubes had been solution-treated at 1433 K for 3 min, and cooled to 1333 K at about 10 K/s, then water-quenched (> 100 K/s).

2.2 Sample preparation and transmission electron microscopy

Small sheets were cut from the tubes at half-thickness, parallel to the longitudinal axis. The sheets were then ground down to a thickness of 100 μm. 3 mm diameter discs were punched from the sheets and further ground until a thickness of 50 μm was reached.

Wt%	C	Si	Mn	P	S
Tube A and B	0.011	0.24	1.68	0.016	0.002
Tube C	0.013	0.25	1.68	0.015	0.002
	Cr	Ni	Mo	B	N
	25.04	21.87	2.15	0.0027	0.124
	24.91	22.04	2.14	0.0027	0.117

Table 1: Composition of the tubes provided by KST, tube A and B are different heats of the same charge of ingot.

Electropolishing was carried out in a Struers Tenupol-5, using a solution of 5% perchloric acid in butoxyethanol, at a voltage of 60 V.

For each tube, thin foils were prepared from three different areas, in some cases more than one foil of the same area was studied.

Microscopy was carried out in a FEI Tecnai F20-G2 fitted with a Gatan Imaging Filter. The acceleration voltage was 200 kV. Results are presented as jump ratio images (for a review of the EFTEM technique, see for example [10]). Details of the edges used, width of the energy window, *etc.* are given in Appendix. Composition profiles across the features of interest are shown that correspond to the length of selected areas in the images. These profiles are averaged over the width of the selected area. Being jump ratio images, the vertical axis of the profiles presented in figure 1, 3, 4 is unitless.

3 Results

3.1 Overview

A total of four thin-foils was studied for tube C, allowing to follow more than 15 grain boundaries. Nevertheless, no precipitates were found in any of the foils.

Four thin-foils were investigated for tube A. Of all the grain boundaries observed, only one was decorated with precipitates. One additional precipitate was observed at a triple

point. Composition and morphology are presented in the next section, as they were found to be identical in all cases.

Precipitates were found in the four thin-foils observed for tube B, however on only a small fraction of the visible grain boundaries.

3.2 Precipitate characteristics

With the exception of the triple point precipitate, most of the particles observed were 15-30 nm thick, with a length 5 to 10 times their thickness, very similar to those reported by Karlsson and Nordén [7].

Figure 1 shows the composition maps for the triple point precipitate. The composition of other precipitates was identical. These maps clearly indicate a strong presence of chromium and possibly some iron. Maps for C, Mn, Mo did not reveal any re-distribution of these elements. Karlsson and Nordén [7] reported similar compositions for tetragonal M_2B. Carbon enrichment was never observed in the precipitates.

Independent investigations [11] using energy dispersive X-ray analysis reported a substitutional composition in agreement with the present results, with the exception of a significant Mo content: 73.5 Cr, 13.4 Fe, 1.5 Ni, 11.5 Mo.

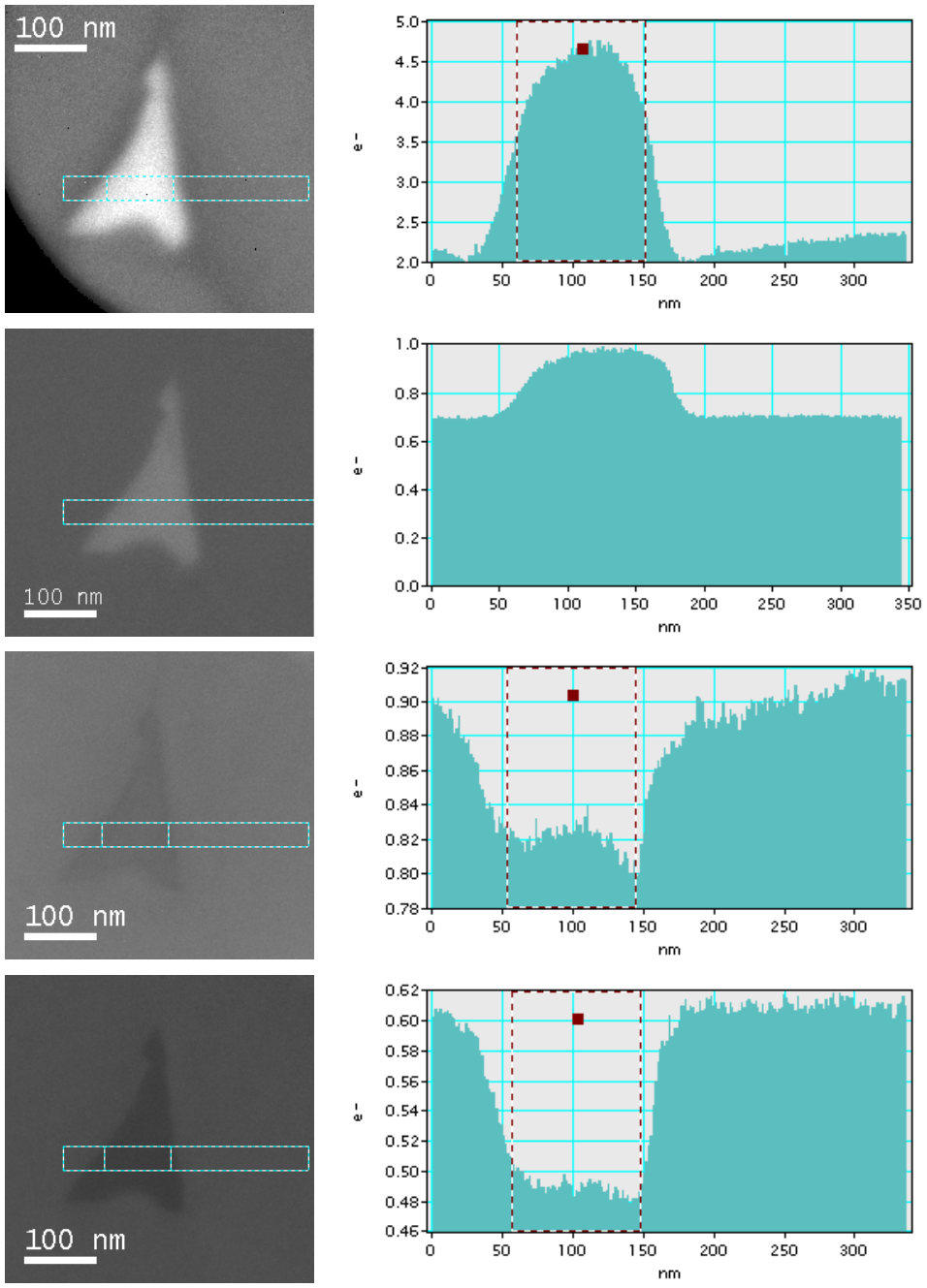

Figure 1: From top to bottom: Cr, B, Fe and Ni jump ratio images of the triple point precipitate found in tube A. Maps for Mo, Mn and C did not reveal any re-distribution.

Figure 2 shows a grain boundary decorated with precipitates in tube B. Localised, strong chromium depletion was systematically observed in the vicinity of the particles, as shown in figure 3.

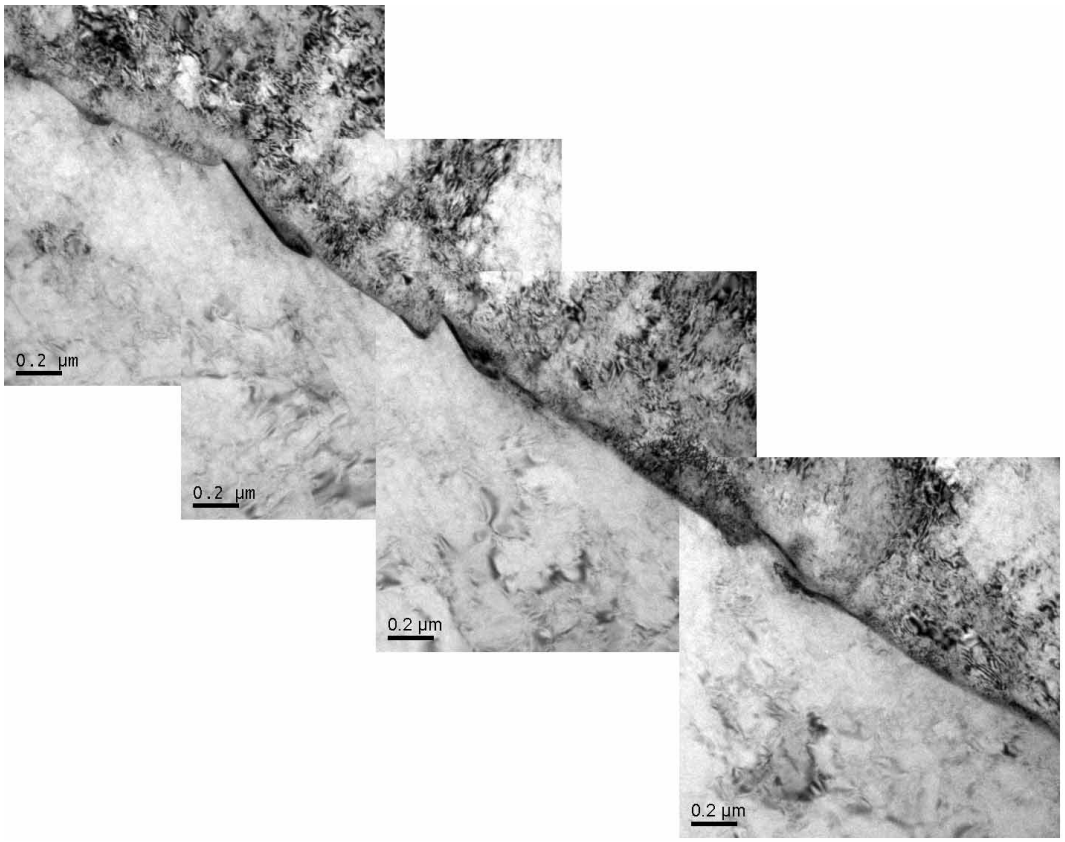

Figure 2: Chromium borides on a grain boundary in tube B.

The asymmetry in the chromium profile was observed for all precipitates, although with some variations in its amplitude. Similar observations have been reported in the case of $M_{23}C_6$ precipitation in 304, and attributed to the grain boundary migration occurring during growth [12] of the precipitate.

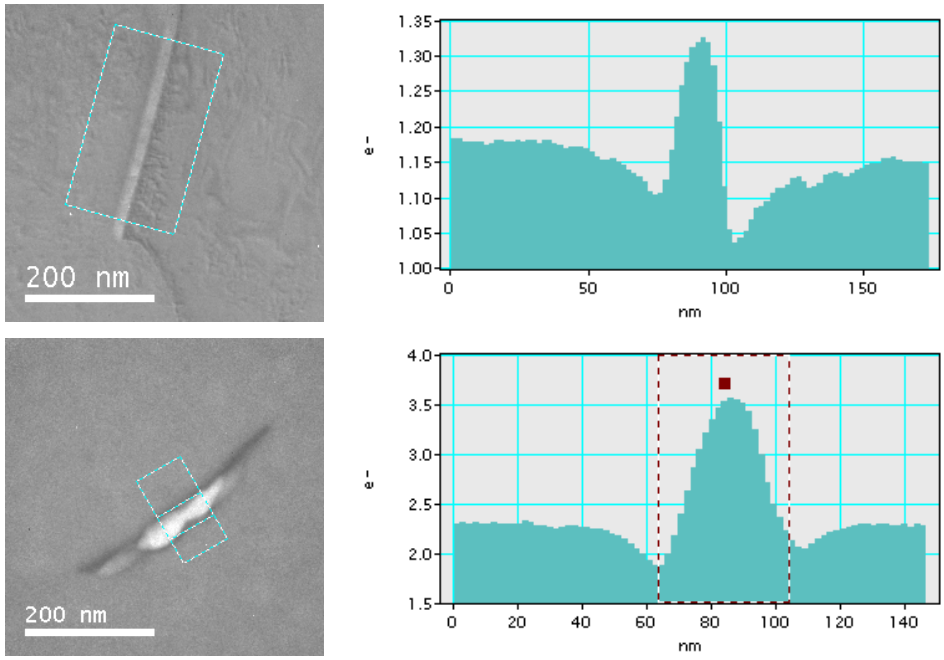

Figure 3: Two examples showing localised depletion with asymmetric chromium concentration profiles.

4 Discussion

As discussed in the introduction, boron segregation can be of two types, which have different characteristics. In a study of type 316L, Karlsson *et al.* [3, 8] reported mainly non-equilibrium segregation of boron for starting temperature (temperature from which the material is quenched) from 1348 to 1523 K, with cooling rates up to 530 K/s. Only lower starting temperatures (1073 K) and high cooling rates (600 K/s) resulted in equilibrium segregation.

Both values of cooling rates reported by KST fall clearly in a region where Karlsson *et al.* identified mainly non-equilibrium segregation. Independent experiments on the effect of starting temperature have confirmed the non-equilibrium nature of boron segregation in this steel [11].

Karlsson and Nordén [7] reported no precipitation for a cooling rate of 530 K/s and precipitates of only $\approx$ 1 nm for 31 K/s. For a cooling rate of 13 K/s, the morphology and size of the precipitates were similar to those reported in the present study. This suggests

that the precipitates observed in the present material most likely formed during the first part of the heat-treatment (1433 K to 1333 K at 10 K/s), rather than during the second part (water quenching from 1333 K). However, in contrast to the results reported in [7], the density of precipitates was not identical on all grain boundaries.

As non-equilibrium segregation is generally believed to affect similarly most grain boundaries, regardless of their degree of misorientation [3, 13], it is not straightforward to explain the present precipitation behaviour. Karlsson *et al.* [7] suggested that grain boundary orientation might become the main factor controlling nucleation when the supersaturation in B is small. The present results support this hypothesis, particularly since boron segregation was observed on some grain boundaries otherwise precipitate free, as illustrated in figure 4.

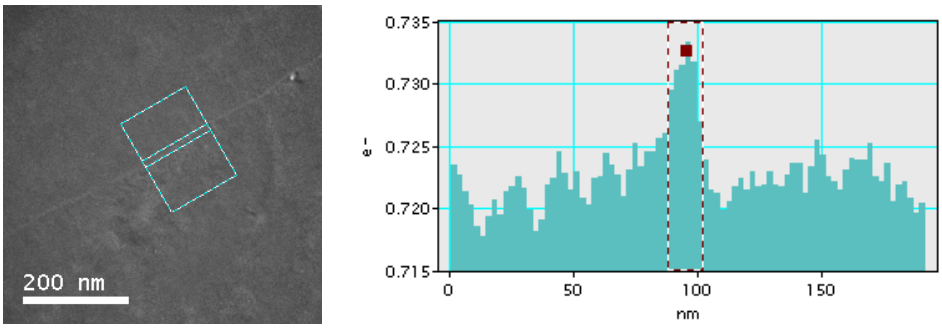

Figure 4: Boron map and profile across a grain boundary, showing segregation of boron.

To further assess the validity of this hypothesis, the nucleation rate was estimated for the formation of M_2B on grain boundaries. Following the classical theory for nucleation [14], the nucleation rate is given by:

$$I = N \exp\left(-\frac{G^*}{RT}\right) \nu \exp\left(-\frac{G_t^*}{RT}\right) \tag{1}$$

where ν is an attempt frequency, often taken as being kT/h , N a number density of nucleation sites and G_t^* the activation energy for transfer of atoms across the interface of the precipitate. In the case of grain boundary nucleation, G^* is given by:

$$G^* = \frac{4}{27} \frac{\{\eta_{\gamma\beta}\,\sigma_{\gamma\beta} - \eta_{\gamma\gamma}\,\sigma_{\gamma\gamma}\}^3 {v_\beta}^2}{{\eta_\beta}^2 \left(\Delta G_m^{\gamma\rightarrow\gamma+\beta}\right)^2} \tag{2}$$

where $\sigma_{\gamma\gamma}$, $\sigma_{\gamma\beta}$ are the interfacial energies for the grain boundary and the interface precipitate-matrix respectively (γ referring to the matrix and β to the precipitate). v_β is the molar volume of the precipitate, and $\Delta G_m^{\gamma\rightarrow\gamma+\beta}$ the driving force for precipitation. $\eta_{\gamma\gamma}$, $\eta_{\gamma\beta}$ are shape factors which relate the area of the interfaces $\gamma:\gamma$ (*i.e.* the surface of grain boundary removed by the nucleation process) and $\gamma:\beta$ (the surface of the matrix-precipitate interface) to the radius of the particle, while η_β is a shape factor for the volume of the precipitate. Details of the values for a spherical cap can be found, for example, in [14].

The driving force for precipitation of M_2B was calculated using the thermodynamic software MT-DATA [15] together with the NPL Plus and SGTE substances databases. It should be emphasised that the following discussion being qualitative, it would hold regardless of which exact boride (M_2B, M_3B_2 or M_5B_3) is used in the calculation, a lower driving force would, for example, simply shift the curves to the right.

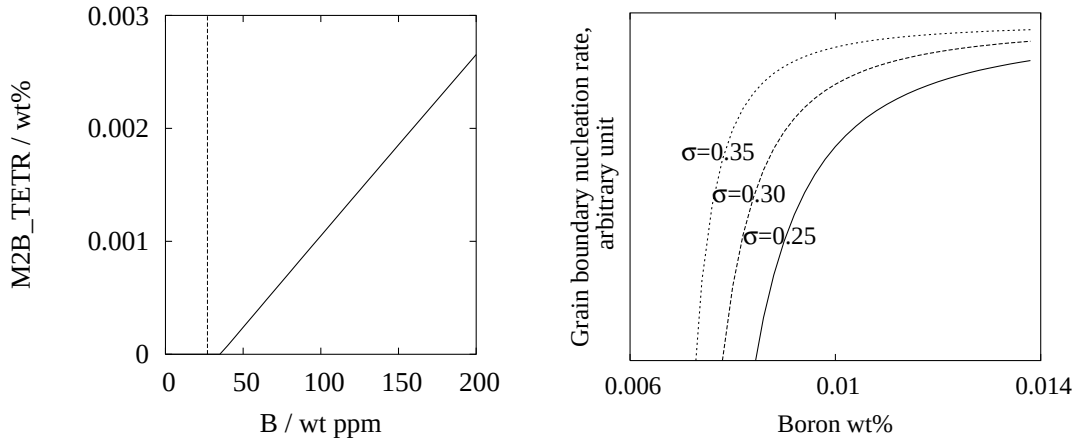

Figure 5: Predicted mass fraction of M2B_TETR and grain boundary nucleation rate as a function of boron content for three different values of grain boundary energies. Driving force calculated with MT-DATA. Other parameters taken as: $G_t^* = 2.5 \times 10^5$ J.mol^{-1}, $\sigma_{\gamma\beta} = 0.23$ J.m^{-2}, $\theta = 30°$ (contact angle) and $v_\beta = 6 \times 10^{-6}$ m^{-3}.

Figure 5 shows the nucleation rate on grain boundaries as a function of boron content, at 1433 K, for three different values of grain boundary energy. For bulk boron content (0.0027 wt%), M_2B is not predicted to be stable. Clearly, at lower boron concentration,

the nucleation rate sensitivity to the grain boundary energy is very large, while at higher boron concentrations, nucleation will happen on most grain boundaries with similar rates. This is entirely consistent with the observation made by Karlsson *et al.* that, for higher boron steels, precipitates are found with similar densities on all grain boundaries, while more irregularly distributed for lower boron content.

Note that the choice of 1433 K for the calculation is for simplicity. Given that significant growth occurs, nucleation must happen close to 1433 K in the temperature range 1333-1433 K, but cannot, in theory, happen at 1433 K where B segregation has not yet taken place. Choosing a different temperature would not affect this qualitative analysis in that the nucleation rate would remain very strongly dependent on σ at low supersaturation.

5 Summary and conclusions

Chromium borides precipitates were observed in a modified type 310 steel with 0.0027 wt% boron, on a small number of grain boundaries. They were found to be composed mostly of chromium and boron, incorporating little if any carbon or substitutional elements. To the extent of the literature covered, these precipitates have not previously been reported in this type of steels.

Comparison with published results suggests that the chromium borides form as a consequence of non-equilibrium segregation of boron to grain-boundaries, during the first part of the heat-treatment. Although this type of segregation is not affected by the nature of the grain boundaries, the non-uniform density of precipitation can be explained if the nucleation rate is considered: if the boron concentration is near the solubility limit, the nucleation rate is very sensitive to the grain boundary interfacial energy. The differences between grain boundaries blurs as the boron content is increased.

The observation of chromium borides on only a small fraction of grain boundaries can therefore be consistent with non-equilibrium segregation. In fact, segregation could be directly observed on some precipitate-free boundaries.

6 Acknowledgements

The authors are gratuful to Professor D. J. Fray for the provision of laboratory facilities at the University of Cambridge, to FEI and the Isaac Newton Trust for provision of the microscope, and to Professor H. K. D. H. Bhadeshia for helpful comments.

Appendix

Elt-edge	Energy (eV)	Pre-edge (eV)	Post-edge (eV)	Width (eV)
Cr-L	575	555	600	30
Mo-M	227	212	247	20
Ni-L	855	830	875	40
Mn-L	640	620	665	30
C-K	284	272	294	20
B-K	188	176	198	20

Table 2: Experimental parameters for acquisition of jump ratio images. Objective aperture size 8.5 mrad.

References

[1] S. K. Banerji, J. E. Morral (Eds.), Boron in austenitic stainless steels, The Metallurgical Society of AIME, Warrendale, 1980.

[2] R. V. Nandedkar, W. Kesternich, Metall. Trans. A 21A (1990) 3033–3038.

[3] L. Karlsson, H. Nordén, H. Odelius, Acta Metall. 36 (1988) 1–12.

[4] S. Shenhua, X. Tingdong, Y. Zhexi, Y. Zongsen, Acta Metall. Mater. 39 (5) (1991) 909–914.

[5] W. Chen, M. C. Chatuverdi, N. L. Richards, G. McMahon, Metall. Mater. Trans. A 29A (1997) 1947–1954.

[6] R. W. Ballufi, Metall. Trans. A 13A (1982) 2069–2075.

[7] L. Karlsson, H. Nordén, Acta Metall. 36 (1988) 35–48.

[8] L. Karlsson, H. Nordén, Acta Metall. 36 (1988) 13–24.

[9] L. Karlsson, Acta Metall. 36 (1988) 25–34.

[10] P. J. Thomas, P. A. Midgley, Topics in catalysis 21 (4) (2002) 109–138.

[11] T. Okuda, personal communication.

[12] S. R. Ortner, A STEM study of the effect of precipitation on grain boundary chemistry in AISI 304 steel, Acta Metall. Mater. 39 (3) (1991) 341–350.

[13] K. Kurzydlowski, R. A. Varin, K. Tangri, Z. Metallkd. 7 (1989) 469–475.

[14] J. W. Christian, Theory of Transformation in Metals and Alloys, Pergamond Press, Oxford, 1975.

[15] National Physical Laboratory, Teddington, Middlesex, UK, MT-DATA Handbook, Utility Module.